High performance charge-transfer induced homojunction photodetector based on ultrathin ZnO nanosheet

Yang Wang, Peng Wang, Yuankun Zhu, Jinrao Gao, Fan Gong, Qing Li, Runzhang Xie, Feng Wu, Ding Wang, Junhe Yang, Zhiyong Fan, Xianying Wang, and Weida Hu 🆔

View Online   Export Citation   CrossMark

ARTICLES YOU MAY BE INTERESTED IN

High quantum efficiency mid-wavelength infrared type-II InAs/InAs$_{1-x}$Sb$_{x}$ superlattice photodiodes grown by metal-organic chemical vapor deposition
Applied Physics Letters 114, 011104 (2019); https://doi.org/10.1063/1.5058714

Carrier localization structure combined with current micropaths in AlGaN quantum wells grown on an AlN template with macrosteps
Applied Physics Letters 114, 011102 (2019); https://doi.org/10.1063/1.5063735

Terahertz read-only multi-order nonvolatile rewritable photo-memory based on indium oxide nanoparticles
Applied Physics Letters 114, 011105 (2019); https://doi.org/10.1063/1.5051029

High performance charge-transfer induced homojunction photodetector based on ultrathin ZnO nanosheet

Yang Wang,[1,2] Peng Wang,[2,a)] Yuankun Zhu,[1] Jinrao Gao,[1] Fan Gong,[2] Qing Li,[2] Runzhang Xie,[2] Feng Wu,[2] Ding Wang,[1] Junhe Yang,[1] Zhiyong Fan,[4] Xianying Wang,[1,3,a)] and Weida Hu[2,a)] (iD)

AFFILIATIONS

[1] School of Materials Science and Engineering, University of Shanghai for Science and Technology, Shanghai 200093, China
[2] State Key Laboratory of Infrared Physics, Shanghai Institute of Technical Physics, Chinese Academy of Sciences, Shanghai 200083, China
[3] Shanghai Innovation Institute for Materials, Shanghai 200444, China
[4] Department of Electronic and Computer Engineering, The Hong Kong University of Science and Technology, Clear Water Bay, Kowloon, Hong Kong, China

[a)] Authors to whom correspondence should be addressed: wdhu@mail.sitp.ac.cn; xianyingwang@usst.edu.cn; and w_peng@mail.sitp.ac.cn

ABSTRACT

Nanostructured zinc oxide (ZnO) semiconductors have emerged as promising materials for high-performance photodetectors due to their natural direct bandgap and extraordinary physicochemical properties. However, the oxygen vacancy defects of nano-ZnO can easily trap oxygen molecules in air and generate charge transfer at the interface, which induced continuous photoconductance that limited the development and application of ZnO in photodetection. Here, we demonstrate a homojunction ultrathin ZnO nanosheet photodetector with high performance and propose a better dominant photoresponse mechanism of the ZnO nanosheet driven by the charge transfer induced local field. The strong localized electric field significantly accelerates the separation of photo-generated carriers and effectively suppresses the dark current. Thus, the photodetector of the charge transfer induced homojunction exhibits ultra-low dark current (10^{-12} A), ultra-high specific detectivity (up to $\sim 10^{14}$ Jones), and fast rising (300 ms) and decaying times (310 ms), taking advantages of high-performance and fast response speed and subverting the limitation of traditional ZnO photodetectors in the field of application. An easy-fabrication, fast response, and high-performance photodetector proposed here provides a good paradigm for the next-generation photodetectors based on two-dimensional nanostructures.
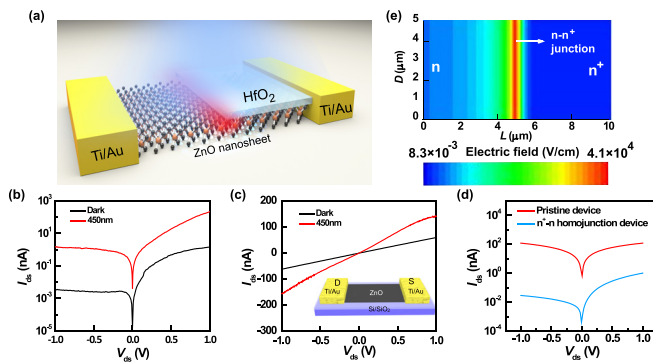
Published under license by AIP Publishing. https://doi.org/10.1063/1.5063611

Nanostructured semiconductor materials (NSMs) have attracted extensive attention due to their excellent physicochemical properties and complex structural characteristics, expecting broad application potency in many fields, such as photodetectors, solar cells, transistors, and energy storage and generation.[1–8] With the advancement of material fabrication techniques, the NSM family is expanded to many unique nanomaterials, such as nanowires,[9–11] nanorods,[12] nanoribbons,[13] and nanosheets.[14] In particular, nanostructured ZnO semiconductors have an intrinsic bandgap of 3.4 eV with a large specific surface area, and they are promising candidates in the field of photodetection applications.[14,28] However, the active surface interactions with oxygen molecules and some intrinsic defects dominate the photoresponse of ZnO nanostructures, and the defect states tend to trap photo-generated electrons and release them slowly, leading to the persistent photoconductivity in ZnO-based photodetectors, which greatly limit the practical application of ZnO in photodetection.[15,16,18] It is known that nanostructured ZnO photodetectors exhibit a very long recovery time of the drain-current after light is turned off because the metal oxide semiconductor is difficult to achieve p-type doping with the presence of many oxygen vacancy defects.[26,27] Therefore, an easy-fabrication, fast response, and high-performance photodetector is desired for next-generation photodetectors based on nanostructured ZnO.

In this work, an advanced homojunction ZnO nanosheet photodetector driven by a charge-transfer induced local field is proposed. By constructing a semi-covered structure, an electron concentration gradient is formed at the interface, thereby forming an n-n$^+$ homojunction. The charge transfer induced built-in electric field can accelerate the separation of electron-hole pairs to increase the photodetection performance with detectivity up to ∼10^{14} Jones and the dark current down to 10^{-12} A, and thus, the signal-to-noise ratio (SNR) of the device is significantly improved. Therefore, our device solves the bottleneck problem to balance the two aspects of high performance and fast response (∼0.3 s) of ZnO photodetectors, which restricts the application of nano-ZnO in photodetection. Overall, this work provides an effective configuration for achieving high-performance optoelectronic devices based on ZnO nanosheets and also demonstrates a very effective method towards the development of homojunction devices based on 2D materials.

Figure 1(a) displays the schematic illustration of the ZnO nanosheet photodetector. Meanwhile, the corresponding photomicrograph and SEM images are shown in Fig. S3 (supplementary material). In order to fabricate the photodetector device, we transfer ZnO nanosheets to the Si/SiO$_2$ substrate and prepare the Ti/Au electrodes by the e-beam lithography, and then, half of the channel was covered with the HfO$_2$ thin film for realizing construction of the homogenous junction. For full fabrication and characterization details, see supplementary material. Interestingly, an evident rectifying characteristic curve of the I$_{ds}$–V$_{ds}$ is observed as the channel is half-covered with the HfO$_2$ thin-film, as shown in Fig. 1(b). Our device shows an ultra-low dark current (3.5×10^{-12} A) in the off-state, and the rectification ratio is more than 400 at $|V| = 1$V, which demonstrate the formation of a decent barrier contributed from the half-covered structure. A device without HfO$_2$ (pristine device) is also fabricated for comparison, and the I$_{ds}$–V$_{ds}$ curves of the pristine device represent a relatively high (6×10^{-8}) dark current at V$_{ds}$

= 1V with good Ohmic contact. In addition, we conducted the transfer characteristic measurement of the pristine device, and the result exhibits a typical n-type semiconductor feature with an effective field-effect mobility of 609 cm^2 V^{-1} s^{-1} (see Fig. S4, supplementary material). To further demonstrate the rectification characteristics of the ZnO n-n$^+$ homojunction device, we perform detailed simulations using Sentaurus TCAD. The simulated I$_{ds}$–V$_{ds}$ characteristics of a pristine device and a n-n$^+$ homojunction device using commercial simulation package of SDEVICE are shown in Fig. 1(d), in which we can see that the simulated I$_{ds}$–V$_{ds}$ curves and experimental results match pretty well. The simulated electric field contour plots for the n-n$^+$ homojunction device using TCAD are shown in Fig. 1(e). We can clearly see that the peak electric field is around 4.1×10^4 V/cm in the n-n$^+$ junction region.

Figure 2(a) displays the output characteristic curves of the half-covered ZnO photodetector at different incident power densities. The photocurrents monotonically increase with the light illumination, and they reach remarkably up to 1.76 μA at the incident power density of 28.775 mW/cm^2 at 450 nm. Under the same condition, a high light on-off ratio of I$_{light}$/I$_{dark}$ ≈ 10^3 is obtained at the bias voltage ∼1V. As shown in Fig. 2(b), the photocurrent increases with the increase in the optical power, and its expression is as follows:
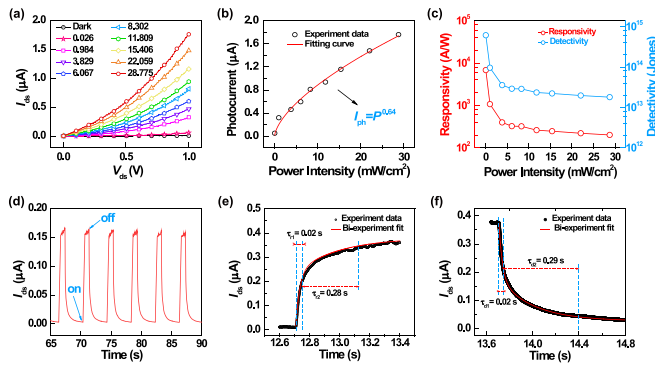
$$I = cp^k, \qquad (1)$$

where I is the photocurrent, P is the optical power, c is a proportionality constant, and k is an empirical fitting value. Based on the results of the curve fittings, we can obtain $c = 0.21$ and $k = 0.64$, showing a sublinear behavior. These results depend on the complex processes of electron-hole generation. Photo-generated carriers can come from the extrinsic transition based on trap states. Nevertheless, the number of trap states is limited. As power intensity increases, more photo-generated charge carriers are trapped, and the photocurrent becomes saturated with the states full filled, which has been reported in many 2D materials.[19,20,25] For practical applications, responsivity (R) and specific detectivity (D*) are often used to characterize the sensitivity of photodetectors, and the responsivity (R) can be expressed as follows:

$$R = \frac{I_{ph}}{P_{opt}S}, \qquad (2)$$

where I$_{ph}$ is the photocurrent, P$_{opt}$ is the incident power density, and S is the effective illuminated area of the device. Assuming that shot noise from the dark current is the major noise source, the specific detectivity (D*) can be calculated by the following equation:

$$D^* = \frac{R}{(2eI_{dark}/S)^{1/2}}, \qquad (3)$$

where e is the electric charge on a single electron and I$_{dark}$ is the dark current. Figure 2(c) presents the calculated R and D* under the condition of different incident power densities. R and D* of the device are up to 6.83×10^3 A W^{-1} and 6.11×10^{14} Jones at V$_{ds}$ = 1V at the power density of 26 μW cm^{-2}, which is larger than that of most ZnO photodetectors (see Table S1, supplementary material). A high photoresponse in the ZnO below the bandgap

FIG. 1. (a) Schematic illustration of the individual ultrathin ZnO nanosheet based photodetectors with a thin HfO$_2$ layer covering one side of the ZnO nanosheets. (b) The I$_{ds}$-V$_{ds}$ characteristics of the homojunction device on the condition of dark and 450 nm illumination. (c) The I$_{ds}$-V$_{ds}$ characteristics of the pristine device in dark and under 450 nm illumination. Inset: Schematic illustration of the pristine device. (d) Simulated semilogarithmic scale I$_{ds}$-V$_{ds}$ characteristics of the pristine device and the n-n$^+$ homojunction device. (e) Simulated electric field contour plot for the n-n$^+$ homojunction device. *L* and *D* are the length and width of the device, respectively.

FIG. 2. (a) The I_{ds}-V_{ds} characteristics under the illumination of light with different incident power densities (mW cm^{-2}). (b) and (c) The photocurrent responsivity and detectivity as a function of incident power density, respectively. (d) Stability test of the device under the reproducible on/off switching of the light. (e) The rise of the current (black line) and bi-exponential fitting (red line) curve of the detector. (f) Recovery current (black line) and the bi-exponential fitting (red line) curve of the detector.

energy is attributed to the high photogain.[23–25] It also can be seen that R and D* of photodetectors decrease with the increasing incident power density, which is not only owing to the saturated absorption of the ZnO channel as the power increases but also caused by the photoexcited electrons induced screening effect in the conduction band of ZnO.[19,26]

We further conducted the time-resolved photoresponse measurement by periodically switching a laser as shown in Fig. 2(d). The photocurrent increases to 1.7 µA as the laser is turned on and then dramatically decreases to its initial state as the light is switched off. Furthermore, the signals exhibit a great repeatability after multi-operation cycles as depicted in Fig. 2(d), indicating a good stability and reliability of the photodetector. Figures 2(e) and 2(f) display the complete rising and falling edges of the device, respectively. Obviously, the behaviors of photocurrent rise and decay involve two processes, including rapid current change and then slow relaxation. The two bi-exponential function equations (4) and (5) used for characterizing the rising and decaying photocurrent, respectively, are

$$I(t) = I_0 + A_1(1 - e^{-t/\tau_{r1}}) + A_2(1 - e^{-t/\tau_{r2}}), \quad (4)$$

$$I(t) = I_0 + A_3 e^{-t/\tau_{d1}} + A_4 e^{-t/\tau_{d2}}, \quad (5)$$

where I_0 is the dark current, and A_1, A_2, A_3, and A_4 are the positive constants. τ_{r1}, τ_{r2} and τ_{d1}, τ_{d2} are time constants for rising and decaying photocurrents, respectively. On the basis of the curve fittings, the calculated rise time constants are $\tau_{r1} = 0.02$ s and $\tau_{r2} = 0.28$ s, and the decay times are $\tau_{d1} = 0.02$ s and $\tau_{d2} = 0.29$ s. In addition, the response speed of the free-state ZnO photodetector is about tens of seconds, which is much slower than that of half-covered ZnO homojunction photodetectors. In comparison, our device exhibits a better repeatability and faster response speed than those of the previously reported typical ZnO photodetectors because HfO$_2$ not only acts as the passivation layer but also induces the build-in electric field (see Fig. S5 and Table S1, supplementary material). Interestingly, we found
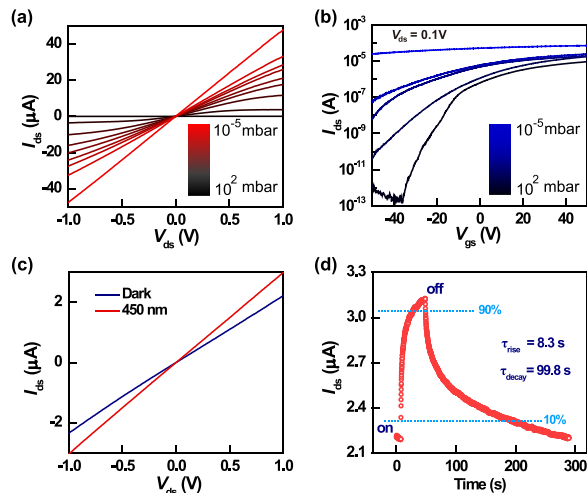
that our device has a good response under the illumination of 520 and 637 nm which is beyond the bandgap limitation of ZnO (i.e., ∼3.3 eV, ∼370 nm) (see Fig. S6, supplementary material).[17,22] It can be explained that O vacancies or Zn interstitials introduce impurity states in the forbidden band as observed in PL characterization and absorption characterization (see Fig. S7, supplementary material). In addition, the n-n$^+$ homojunction device exhibits good responsivity and fast photoresponse speed under the consideration of 375 nm illumination as shown in Figs. S8(a) and S8(b) (supplementary material).

To accurately examine the spatial distribution of the electric field of the ZnO homojunction, we conducted the two-dimensional photocurrent imaging measurement. Figure 3 shows the photocurrent mapping results under the condition of 450 nm laser with the power density of 28.775 mW cm^{-2}. Brightest regions in each figure reveal that the photocurrents are mainly generated at the interface between the bare ZnO and HfO$_2$ capped region, which implies that an effective charge-transfer induced built-in electric field is established in the ZnO homojunction. In addition, the rapid separation of photogenerated carriers driven by the built-in electric field contributes greatly to the fast response of the device. In the dark, the oxygen is absorbed by the surface of the nanosheet and then captures the electrons (O$_2$+2e$^-$→O^{2-}). Under illumination, the photogenerated holes are migrated to the surface due to energy bands bending upwards and then neutralize the atomic oxygen radical anion (h$^+$+O^{2-}→O$_2$). In the following, the ZnO nanosheet releases the oxygen. Nevertheless, the photo-generated electrons contribute to the photocurrent until the oxygen is absorbed and ionized again. As for the region covering HfO$_2$, the oxygen concentration in the region covering HfO$_2$ is lower so that the process (O+ 2e$^-$→O^{2-}) is slowed down. It is available to achieve high photogain by means of efficiently separating the photoinduced electron-hole pairs and increasing the lifetime of carriers. Therefore, a weak photocurrent is generated in the region covering HfO$_2$.
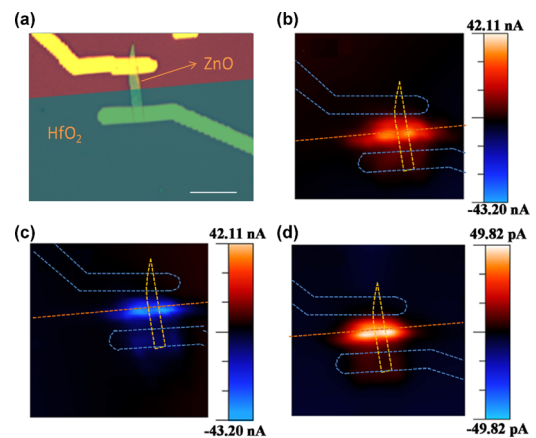
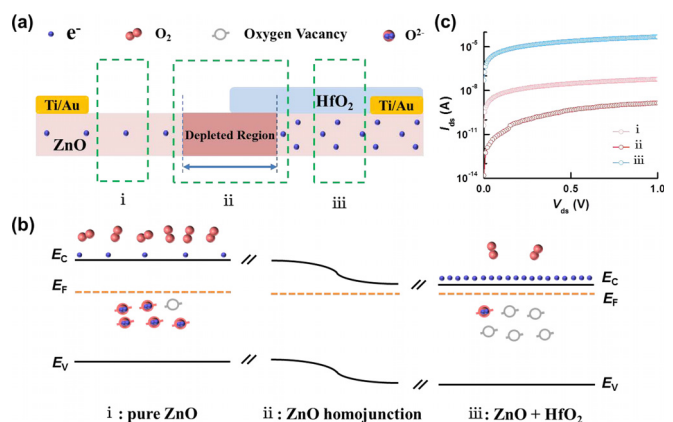**FIG. 3.** (a) Optical microscopy image; the scale bar is 10 µm. (b), (c), and (d) Photocurrent mapping images of the homojunction photodetector under a 450 nm laser excitation with $V_{ds} = -1$ V, $V_{ds} = 1$ V, and $V_{ds} = 0$ V.

To clarify the formation mechanisms of the homojunction, we investigated the effect of oxygen on the charge transfer of ZnO nanosheets. Drain-source (I_{ds}–V_{ds}) plots were measured at different gas pressures which can be controlled by a molecular pump connected to the vacuum probe station. As shown in Fig. 4(a), the current increases almost to three orders as the gas pressure decreases from 10^2 to 10^{-5} mbar. In Fig. 4(b), the threshold voltage of the pristine device shifts to a more negative value with the decreasing gas pressure. When the gas pressure is reduced to 10^{-5} mbar, the gate voltage is unable to effectively modulate the channel conductance of the ZnO nanosheet as before. In comparison, output characteristics of the pristine device at different vacuum degrees in the dark of ZnO device are completely covered by HfO_2 [Fig. S8(c), supplementary material]. It can be seen that the charge density of the ZnO device completely covered by HfO_2 does not change with pressure. In addition, we also measured the drain-current of the ZnO homojunction under the consideration of dark and illumination (450 nm, 28.775 mW cm^{-2}). It is noticed that the ZnO homojunction device shows no rectification characteristic in a vacuum under both illumination and dark [Fig. 4(c)], which indicates that the gas atmosphere plays a key role in the formation of the homojunction. Meanwhile, we also conducted the time dependent photo-response measurement with an applied voltage of 1 V [Fig. 4(d)]. The rising and decaying times are 8.3 s and 99.8 s, respectively. The decrease in the number of oxygen molecules adsorbed in the uncovered HfO_2 region leads to the charge transfer and the disappearance of the homojunction, which significantly slow down the reaction rate. In general, these results indicate that the performance of the device is mainly dominated by the oxygen molecules, and the specific details are discussed below.

Previously reported studies of pure ZnO nanostructure photodetectors exhibited high dark current, low detectivity, and quite long response time (see Table S1, supplementary material) in comparison with the homojunction ZnO photodetector demonstrated in this work whose performance is enhanced by the charge-transfer dependent photoresponse mechanism. For achieving the ZnO nanosheet homojunction, we use a thin HfO_2 film deposited onto half of the ZnO nanosheet to prevent the oxygen vacancies from adsorbing the oxygen molecules, utilizing the effect of charge transfer in the ZnO channel and forming a carrier concentration gradient at the interface [Fig. 5(a)]. For a ZnO photodetector, oxygen vacancies play an important role in manipulating the conductance of the device.[15,21] As for the pristine device in the atmospheric environment, the oxygen vacancies in the ultrathin ZnO nanosheets tend to adsorb oxygen molecules in the air and capture electrons to form oxygen ions (O^{2-}). The adsorption process can be expressed as follows: $O + 2e^- \rightarrow O^{2-}$ [Fig. 5(b)-i], and thus, the carrier concentration in the conduction band decreases with the Fermi level far away from the conduction band, resulting in a smaller dark current of the ZnO nanosheet device in the atmospheric environment. Upon illumination, some of the photogenerated electrons are captured by the adsorbed oxygen,[18] and the releasing processes are quite slow, leading to the long recovery time as the illumination cut off. Further, we built the HfO_2 covered structure to prevent the air in the chamber in order to simulate a similar vacuum environment as shown in Fig. 5(b)-iii. As the pressure decreases, the concentration of oxygen remaining in the chamber is so low that the number of oxygen molecules adsorbed on the ZnO nanosheet decreases. At this point, the increased concentration of oxygen vacancies in the ZnO nanosheet contribute to an additional forward gate voltage in comparison of that in the atmosphere, making the Fermi level closer to the conduction band. In this process, the electrons are released from the negatively charged oxygen ions "O^{2-} (ad)" via the following reaction $O^{2-} \rightarrow 1/2\,O + 2e^-$. Both the increased gating effect of oxygen vacancies and the released charges transferred to the

FIG. 4. (a) Output characteristics of the pristine device at different vacuum degrees in the dark. (b) Transfer characteristics of the pristine device at different vacuum degrees in the dark. (c) Comparison of the I_{ds}-V_{ds} characteristics of the homojunction photodetector in the dark and illumination in vacuum. (d) The reproducible on/off switching of the ultrathin ZnO nanosheet homojunction photodetector under 450 nm-light illumination (28.775 mW cm^{-2}) in vacuum.

FIG. 5. (a) Schematic diagram of ZnO nanosheet homojunction charge distribution. (b) The carrier transport mechanism of pure ZnO, ZnO homojunction, and ZnO+HfO$_2$. E_F, E_C, and E_V stand for the Fermi level, the minimum conduction band energy, and the maximum valence band energy, respectively. (c) Comparison of the I_{ds}-V_{ds} characteristics of pure ZnO, ZnO homojunction, and ZnO+HfO$_2$ in the dark.

conduction band contribute to the increase in the concentration of the conduction electrons. As shown in Fig. 5(b)-ii, the different electron concentrations of the two sides result in an apparent n-n$^+$ homojunction at the interface in the atmosphere, which can effectively inhibit the dark current and accelerate the separation of photogenerated electron-hole pairs. In addition, the built-in electric field suppresses dark current/carrier density effectively better than the oxygen vacancy modulation effect as shown in Fig. 5(c), indicating that the half-covering structure of our device can easily achieve charge separation in space. Besides, the unique two-dimensional ultrathin structure of the ZnO nanosheet can effectively confine the transport orientation of carriers and as a freeway to facilitate the transport of photogenerated carriers.[29,30] Therefore, fast response speed is achieved for the ZnO nano-sheets photodetector.

In summary, a unique n-n$^+$ homojunction ZnO nanosheet photodetector is fabricated by covering half of the channel with the HfO$_2$ thin film. With the introduction of charge-transfer induced strong built-in electric field, the photo-generated carriers can be separated rapidly, and the dark current is suppressed effectively, thus improving the device performance and solving the problem of persistent photoconduction in ZnO photodetectors. Particularly, ultralow dark current (10^{-12} A), large responsivity (10^3 A W^{-1}), and high detectivity (10^{14} Jones) are achieved for the next-generation photodetectors based on homojunction nano-ZnO. Taking advantages of high-performance and fast response speed ($\sim$300 ms), the device surpasses the limitation of traditional ZnO photodetectors with potential practical application. In addition, a comprehensive charge-transfer dependent photoresponse mechanism of ZnO homojunction is proposed. This mechanism considers the impact of oxygen vacancy density and the gating effect driven by charge transfer in the ZnO channel, and it provides theoretical support for better oxide semiconductor photodetectors in the future. Since the fabrication of p-type conducting ZnO is still challenging, the idea of homojunction built via charge-transfer modifications provide a good direction for the nano-ZnO applications in photodetection.

See supplementary material for the experimental details, the complete morphology and structural characterization, and their analysis.

REFERENCES

[1] F. P. García de Arquer, A. Armin, P. Meredith, and E. H. Sargent, Nat. Rev. Mater. **2**, 16100 (2017).
[2] F. H. L. Koppens, T. Mueller, P. Avouris, A. C. Ferrari, M. S. Vitiello, and M. Polini, Nat. Nanotechnol. **9**, 780 (2014).
[3] C. Liu, Y. Chang, T. B. Norris, and Z. Zhong, Nat. Nanotechnol. **9**, 273 (2014).
[4] Y. K. Mishra and R. Adelung, Mater. Today **21**, 631 (2018).
[5] M. Buscema, J. O. Island, D. J. Groenendijk, S. I. Blanter, G. A. Steele, H. S. J. van der Zant, and A. castellanos-Gomez, Chem. Soc. Rev. **44**, 3691 (2015).
[6] Z. Y. Fan, H. Razavi, J. Do, A. Moriwaki, O. Ergen, Y. L. Chueh, P. W. Leu, J. C. Ho, T. Takahashi, L. A. Reichertz, S. Neale, K. Yu, M. Wu, J. W. Ager, and A. Javey, Nat. Mater. **8**, 648 (2009).
[7] E. M. C. Fortunato, P. M. C. Barquinha, A. C. M. B. G. Pimentel, A. M. F. Gonçalves, A. J. S. Marques, L. M. N. Pereira, and R. F. P. Martins, Adv. Mater. **17**, 590 (2005).
[8] J. L. Wang, H. H. Fang, X. D. Wang, X. S. Chen, W. Lu, and W. D. Hu, Small **13**, 1700894 (2017).
[9] H. H. Fang, W. D. Hu, P. Wang, N. Guo, W. J. Luo, D. S. Zheng, F. Gong, M. Luo, H. Z. Tian, X. T. Zhang, C. Luo, X. Wu, P. P. Chen, L. Liao, A. L. Pan, X. S. Chen, and W. Lu, Nano Lett. **16**, 6416 (2016).
[10] A. Waleed, M. M. Tavakoli, L. L. Gu, Z. Y. Wang, D. Q. Zhang, A. Manikandan, Q. P. Zhang, R. J. Zhang, Y. L. Chueh, and Z. Y. Fan, Nano Lett. **17**, 523 (2017).
[11] G. Chen, B. Liang, X. Liu, Z. Liu, G. Yu, X. Xie, T. Luo, D. Chen, M. Zhu, G. Z. Shen, and Z. Y. Fan, ACS Nano **8**, 787 (2014).
[12] Z. Y. Fan, D. J. Ruebusch, A. A. Rathore, R. Kapadia, O. Ergen, P. W. Leu, and A. Javey, Nano Res. **2**, 829 (2009).
[13] S. J. Chen, Y. C. Liu, C. L. Shao, R. Mu, Y. M. Lu, J. Y. Zhang, D. Shen, and X. W. Fan, Adv. Mater. **17**, 586 (2005).
[14] H. Z. Tian, X. D. Wang, Y. K. Zhu, L. Liao, X. Y. Wang, J. L. Wang, and W. D. Hu, Appl. Phys. Lett. **110**, 043505 (2017).
[15] J. D. Prades, F. Hernandez-Ramirez, R. Jimenez-Diaz, M. Manzanares, T. Andreu, A. Cirera, A. Romano-Rodriguez, and J. R. Morante, Nanotechnology **19**, 465501 (2008).
[16] Z. Y. Fan, P. C. Chang, J. G. Lu, E. C. Walter, R. M. Penner, C. H. Lin, and H. P. Lee, Appl. Phys. Lett. **85**, 6128 (2004).
[17] C. L. Du, Z. B. Gu, Y. M. You, J. Kasim, T. Yu, Z. X. Shen, Z. H. Ni, Y. Ma, G. X. Cheng, and Y. F. Chen, J. Appl. Phys. **103**, 023521 (2008).
[18] Y. Z. Jin, J. P. Wang, B. Q. Sun, C. B. James, and C. G. Neil, Nano Lett. **8**, 1649 (2008).
[19] W. J. Yu, Y. Liu, H. L. Zhou, A. X. Yin, Z. Li, Y. Huang, and X. F. Duan, Nat. Nanotechnol. **8**, 952 (2013).
[20] W. Zhang, J. K. Huang, C. H. Chen, Y. H. Chang, Y. J. Cheng, and L. J. Li, Adv. Mater. **25**, 3456 (2013).
[21] Z. Y. Fan, D. W. Wang, P. C. Chang, W. Y. Tseng, and J. G. Lua, Appl. Phys. Lett. **85**, 5923 (2004).
[22] Y. K. Zhu, H. Y. Yang, F. Sun, and X. Y. Wang, Nanoscale Res. Lett. **11**, 175 (2016).
[23] G. Konstantatos, M. Badioli, L. Gaudreau, J. Osmond, M. Bernechea, F. P. G. de Arquer, F. Gatti, and F. H. Koppens, Nat. Nanotechnol. **7**, 363 (2012).
[24] S. Jeon, S. E. Ahn, I. Song, C. J. Kim, U. I. Chung, E. Lee, I. Yoo, A. Nathan, S. Lee, K. Ghaffarzadeh, J. Robertson, and K. Kim, Nat. Mater. **11**, 301 (2012).
[25] O. Lopez-Sanchez, D. Lembke, M. Kayci, A. Radenovic, and A. Kis, Nat. Nanotechnol. **8**, 497 (2013).
[26] N. Faraji, C. Ulrich, N. Wolff, L. Kienle, R. Adelung, Y. K. Mishra, and J. Seidel, Adv. Electron. Mater. **2**, 1600138 (2016).
[27] C. Soci, A. Zhang, B. Xiang, S. A. Dayeh, D. P. R. Aplin, J. Park, X. Y. Bao, Y. H. Lo, and D. Wang, Nano Lett. **7**, 1003 (2007).
[28] P. Wang, Y. Wang, L. Ye, M. Z. Wu, R. Z. Xie, X. D. Wang, X. S. Chen, Z. Y. Fan, J. L. Wang, and W. D. Hu, Small **14**, 1800492 (2018).
[29] G. H. Guang, M. Suja, M. G. Chen, E. Bekyarova, R. C. Haddon, J. L. Liu, and M. E. Itkis, ACS Appl. Mater. Interfaces **9**, 37094 (2017).
[30] B. Zhao, F. Wang, H. Y. Chen, Y. P. Wang, M. M. Jiang, X. S. Fang, and D. X. Zhao, Nano Lett. **15**, 3988 (2015).